



City Research Online

City, University of London Institutional Repository

Citation: Kumar, A., Rastogi, V., Agrawal, A. & Rahman, B. M. (2012). Birefringence analysis of segmented cladding fiber. *Applied Optics*, 51(15), pp. 3104-3108. doi: 10.1364/ao.51.003104

This is the unspecified version of the paper.

This version of the publication may differ from the final published version.

Permanent repository link: <https://openaccess.city.ac.uk/id/eprint/1247/>

Link to published version: <https://doi.org/10.1364/ao.51.003104>

Copyright: City Research Online aims to make research outputs of City, University of London available to a wider audience. Copyright and Moral Rights remain with the author(s) and/or copyright holders. URLs from City Research Online may be freely distributed and linked to.

Reuse: Copies of full items can be used for personal research or study, educational, or not-for-profit purposes without prior permission or charge. Provided that the authors, title and full bibliographic details are credited, a hyperlink and/or URL is given for the original metadata page and the content is not changed in any way.

City Research Online:

<http://openaccess.city.ac.uk/>

publications@city.ac.uk

Birefringence analysis of segmented cladding fiber

Ajeet Kumar,^{1,*} Vipul Rastogi,² Arti Agrawal,³ and B. M. A. Rahman³

¹Department of Applied Physics, Delhi Technological University, Delhi-110042, India

²Department of Physics, Indian Institute of Technology Roorkee, Roorkee 247 667, India

³Department of Electrical, Electronics & Information Engineering, School of Engineering and Mathematical Sciences, City University London, EC1V OHB, UK

*Corresponding author: ajeetdph@gmail.com

Received 10 January 2012; revised 29 March 2012; accepted 30 March 2012;
posted 2 April 2012 (Doc. ID 161163); published 18 May 2012

We present a full-vectorial modal analysis of a segmented cladding fiber (SCF). The analysis is based on the H -field vectorial finite element method (VFEM) employing polar mesh geometry. Using this method, we have analyzed the circular SCF and the elliptical SCF. We have found that the birefringence of the circular SCF is very small (1.0×10^{-8}). Birefringence of a highly elliptical SCF can be altered to some extent by the number of segments and duty cycle of segmentation in the segmented cladding. However, the change is not profound. The analysis shows that the circular SCF possesses low birefringence and that the segmented cladding does not add any significant birefringence in an elliptical fiber. This result strongly indicates that small deviations in the segmented cladding parameters arising from fabrication process do not significantly affect the birefringence of the fiber. © 2012 Optical Society of America
OCIS codes: 060.2420, 060.2280, 230.5440, 060.4005.

1. Introduction

Segmented cladding fibers (SCFs), in which the cladding is formed by periodic arrangement of high- and low-refractive index segments in the angular direction have shown potential for large mode area (LMA), single mode (SM) operation. Such a fiber is highly desirable in high-power fiber lasers [1], dense wavelength division multiplexing optical communication systems, and midinfrared sensing [2,3]. SCFs have been fabricated in polymer [4,5] and silver halide glass [3] and have experimentally demonstrated LMA operation. The working principle of the SCF is mode filtering: A high differential leakage loss between the fundamental and the higher order modes along with nominal loss to the fundamental mode ensures effective SM behavior of the SCF. Due to the potential applications of SCF in the aforementioned fields, it is important to study in detail the propagation characteristics of SCF and to explore the effect of

deviations in segmented cladding parameters, which may arise from fabrication process.

The radial effective index method (REIM) has been conventionally used to determine the propagation characteristics in terms of effective index and leakage loss of the modes of an SCF. However, REIM, being a scalar approach, does not reveal information about the polarization-dependent modal properties of the fiber, which is important for applications and devices sensitive to polarization. There have been several studies on the vectorial analysis of the optical fibers [6–13]. In this paper, we carry out a full vectorial analysis of the SCF using the vectorial finite element method (VFEM). VFEM is a well-established method for highly accurate characterization of optical structures [9,13]. For the analysis of SCF presented in this paper, we have used the H -field formulation [13] with a polar mesh. Numerical simulations on circular SCF confirm that it does have a small birefringence ($\sim 10^{-8}$) as predicted earlier [1,2]. We also investigated the effect of the segmented cladding on an already birefringent core. In order to study this, we have considered a small core with an elliptical

1559-128X/12/153104-05\$15.00/0
© 2012 Optical Society of America

cross-section in the SCF. We show that the segmented cladding affects the birefringence of the elliptical fiber to some extent, but the effects are not significant. This shows that the angular segmentation in the cladding does not have a strong effect on the birefringence of the fiber.

2. Finite Element Analysis and Results for the Circular SCF

The transverse cross-section of the SCF is shown in Fig. 1. The fiber consists of a uniform core of refrac-

accurately. Therefore, curved boundaries are represented well, and the stair-casing error associated with finite difference—based algorithms is not encountered. Furthermore, irregular meshing can be employed for better computational accuracy. The H -field formulation developed previously by Rahman and Davies is valid for microwave and optical guided-wave devices, including the increasingly important terahertz frequency range. The H -field formulation with the augmented penalty function technique is given as [13]:

$$\omega^2 = \frac{\left(\int (\nabla \times \vec{H}) * \hat{\epsilon}^{-1} (\nabla \times \vec{H}) d\Omega + \int (\alpha/\epsilon_0) (\nabla \cdot \vec{H}) * (\nabla \cdot \vec{H}) d\Omega \right)}{\int \vec{H} * \hat{\mu} \vec{H} d\Omega} \quad (1)$$

tive index n_1 at the center ($0 < r < a$). The core is surrounded by a segmented cladding formed by alternate high-index (n_1) and low-index (n_2) segments of angular width $2\theta_1$ and $2\theta_2$, respectively, in the region $a < r < b$. The total number of segments, N , satisfies the relation $N(\theta_1 + \theta_2) = \pi$. The index difference between the two media is characterized by $\Delta = \frac{n_1^2 - n_2^2}{2n_1^2}$.

The period and the duty cycle of segmentation are given by $\Lambda = 2\theta_1 + 2\theta_2$ and $\gamma = 2\theta_2/\Lambda$, respectively.

We have analyzed the SCF using the VFEM, which is one of the most powerful and versatile method in many branches of engineering to solve the problems involving complicated geometries. In the finite element approach, the problem domain is divided into smaller subdomains containing elements of different shapes and sizes, such that the boundaries of regions with different dielectric constants are represented

where \vec{H} is the full-vectorial magnetic field; ϵ and μ are the permittivity and permeability, respectively, of the waveguide; ϵ_0 is the permittivity of the free space; ω^2 is the eigen value; and α is a dimensionless parameter used to impose the divergence-free condition of the magnetic field in a least-squares sense. Modes of the SCF have been presented in terms of the transverse magnetic field components, H_{mn}^x and H_{mn}^y , as commonly used for integrated optical waveguide problems, where the subscripts m and n denote the field maxima along the x - and the y -axes, respectively. For the H_{mn}^y mode, which is also known as the quasi-TE mode, the H_y (or E_x) field is dominant compared to the H_x (or E_y) field component. Similarly, for the H_{mn}^x (quasi-TM) mode, the H_x and H_y fields are the dominant and nondominant components, respectively.

As the fiber has two-fold symmetry, only a quarter-section has been considered in the simulation. This allows use of a larger number of elements to represent the structure and obtain higher accuracy. The quarter-section of the SCF under consideration has been divided into many small first-order elements. The size of the element depends upon the number of radial and angular divisions, which in turn determines the accuracy of the simulation. A schematic of the finite element representation of the structure is shown in Fig. 2. To compare the results of the present FEM with scalar REIM, we have divided the quarter segment of the fiber into 90 angular and 165 radial divisions. A good agreement between the two methods is found and is presented in Table 1. We have also plotted the contour plot of the fundamental mode of the SCF at two different wavelengths, as shown in Fig. 3. The periodic variation of the refractive indices in the segments in the cladding region is reflected in the contour plot. High-index segments of the cladding pull the field toward the outer cladding region. After benchmarking the

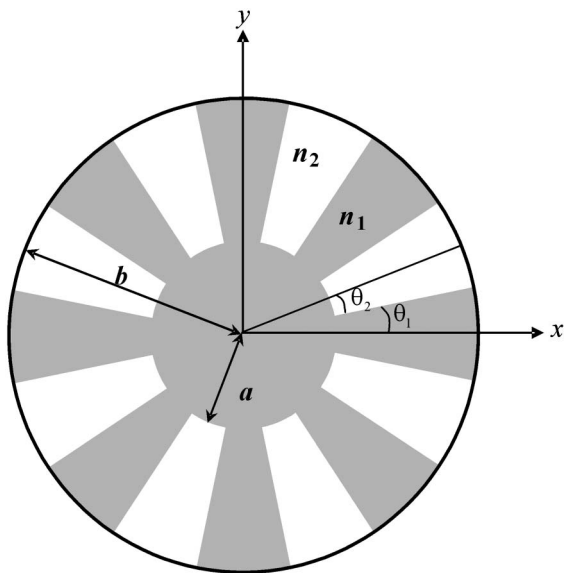


Fig. 1. Transverse cross-section of the SCF.

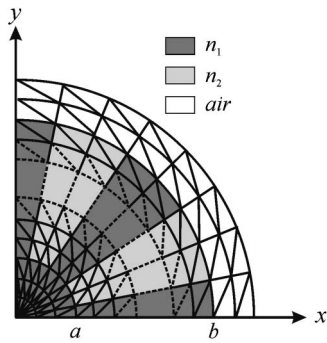


Fig. 2. Finite element representation of a quarter section of the SCF.

results of FEM, we calculated the birefringence of the SCF, which is defined as $B = n_x - n_y$, where n_x and n_y represent the effective indices of the quasi-TE mode (H_{11}^y) and quasi-TM (H_{11}^x) modes, respectively. The SCF considered here has the parameters $a = 10 \mu\text{m}$, $b = 30 \mu\text{m}$, $\Delta = 0.0035$, $N = 8$, and $\gamma = 0.50$. At an operating wavelength of $\lambda = 1550 \text{ nm}$, the birefringence of the fiber is very small (1×10^{-8}), as predicted earlier [1,3]. Since this value of birefringence is extremely small and of the order of computational accuracy we focus on, the study of the birefringence in an elliptical SCF.

3. Elliptical SCF

We investigate an elliptical SCF with ($N = 8$), whose cross-section is shown in Fig. 4. The high-index (n_1) elliptical core of the elliptical SCF is characterized by semimajor and semiminor lengths a and b , respectively, and is embedded in a uniform inner cladding of refractive index n_2 and outer segmented cladding of period, Λ , and duty cycle, γ . The whole structure is enclosed in a jacket of refractive index n_1 . The widths of the uniform, segmented cladding layers along the major axis, are denoted by d_{cl} , d_{scl} , and d_{ex} , respectively. The eccentricity of the parameter of the structure is defined as $e_{clad} = \sqrt{1 - \frac{r_y^2}{r_x^2}}$, where r_x and r_y represent the radial position of the cladding layers along the major and minor axis. e_{clad} remains the same for all the cladding layers.

Table 1. Comparison of Mode Indices of the Segmented Cladding Fiber (SCF) Calculated by Radial Effective Index Method (REIM) and Finite Element Method (FEM) at Different Wavelengths for the Fiber Parameters: $a = 10 \mu\text{m}$, $b = 30 \mu\text{m}$, $\Delta = 0.0035$, $N = 8$, and $\gamma = 0.50$

λ (nm)	Mode Effective Index	
	REIM	FEM
450	1.449397	1.449388
650	1.449324	1.449310
850	1.449230	1.449213
1050	1.449121	1.449103
1350	1.448937	1.448920
1550	1.448807	1.448792
1750	1.448673	1.448660

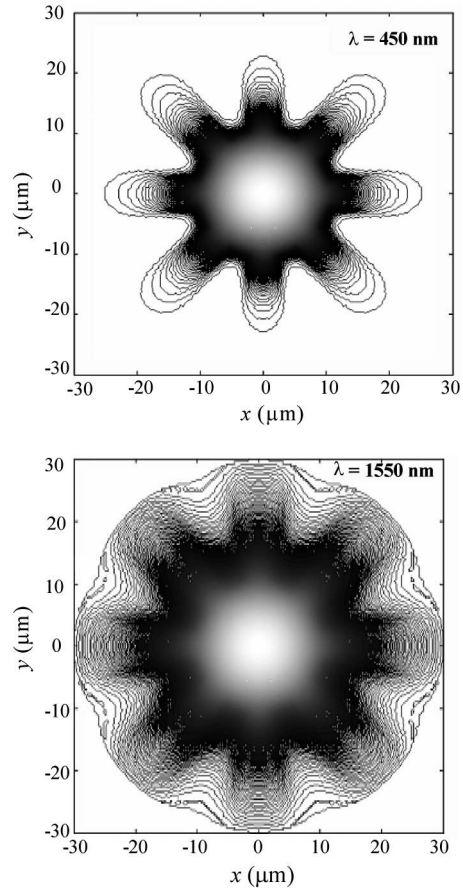


Fig. 3. Contour plot of the fundamental mode at two different wavelengths (450 and 1550 nm) for the parameters defined in Table 1.

The accuracy of the full vectorial finite element method depends on the size of meshing. It is therefore necessary to investigate the convergence of the mode effective index (n_{eff}) with the mesh parameters N_{radial} , the number of divisions in radial directions, and $N_{angular}$, the number of divisions in angular directions. We have carried out a convergence study for fiber parameters: $a = 3.75 \mu\text{m}$, $b = 1.25 \mu\text{m}$, $d_{cl} = 6.25 \mu\text{m}$, $d_{scl} = 20 \mu\text{m}$, $d_{ex} = 5 \mu\text{m}$, and $e_{clad} = 0.87$. Figure 5(a) shows that the value of birefringence saturates as N_{radial} is increased beyond 15. Therefore,

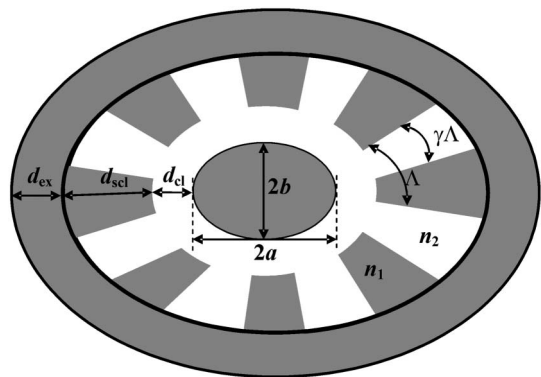


Fig. 4. Transverse cross-section of an elliptical SCF.

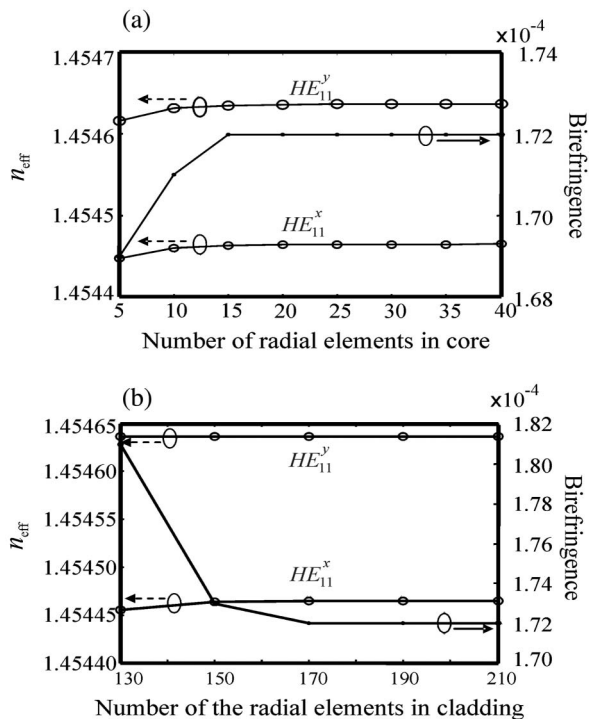


Fig. 5. Effect of mesh parameters on the convergence of effective indices of modes and birefringence for the parameters given by Eq. (2) at $\lambda = 1550$ nm.

it is necessary to take at least 15 radial elements inside the core region to get the accurate value of the effective indices of both the modes. Further increase in N_{radial} does not result in any improvement in the accuracy with which B can be determined. A similar study has also been carried out for the number of radial elements inside the cladding region, and the results are shown in Fig. 5(b). It is clear from the figure that the value of B saturates as the number of elements is increased beyond 170. Therefore, the number of radial elements in the cladding has been clamped to 170.

We also performed a similar convergence study for N_{angular} . We found that $N_{\text{angular}} = 180$ in a quarter-section of fiber, which is sufficient to achieve desired accuracy in n_{eff} .

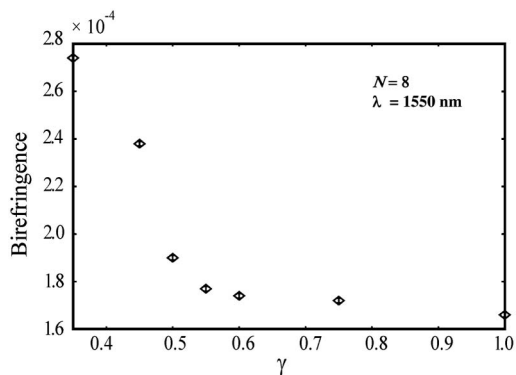


Fig. 6. Effect of duty cycle (γ) on birefringence of elliptical SCF.

4. Birefringence Properties of the Elliptical SCF

We studied the effect of the cladding parameters and the wavelength of operation on the birefringence of the elliptical SCF. In this study, we only considered the geometrical birefringence, as it is much larger than the stress-induced birefringence for the parameters under consideration [8]. We carried out numerical simulations for eight-segment SCF with the following values of various parameters, unless stated otherwise:

$$\begin{aligned} n_2 &= 1.444388, & \Delta &= 1.6\%, & a &= 3.75 \mu\text{m}, \\ b &= 1.25 \mu\text{m}, & d_{\text{cl}} &= 6.25 \mu\text{m}, & d_{\text{scl}} &= 20 \mu\text{m}, \\ d_{\text{ex}} &= 5 \mu\text{m}, & e_{\text{clad}} &= 0.87, \\ N_{\text{angular}} &= 180 & \text{and} & N_{\text{radial}} &= 250. \end{aligned} \quad (2)$$

The birefringence of an elliptical core fiber can be affected by the segmented cladding of the SCF due to its azimuthal asymmetry. The azimuthal asymmetry in the segmented cladding can be controlled by two parameters: (1) Number of low and high segments (N) in the cladding region and (2) the duty cycle of the segmentation (γ). For a fixed value of N , the duty cycle (γ) controls the angular width of the high- and low-index regions in the segmented cladding and thus the proportion of the area of the cladding, which has low refractive index. Thus, a high value of γ implies the overall index in the cladding is lower than for a smaller value of γ . While for a given duty cycle, the number of segments, N , controls the angular width of the high- and low-index regions as well as the distribution of segments as in the cladding. Moreover, the relative field amplitudes in the high-index segments along x - and y - axes are also affected by N . In this way, both the parameters N and γ affect the asymmetry of the fiber, which in turn affects the birefringence. We have studied the effect of these parameters on the birefringence of the designed fiber, and the results are shown in Figs. 6 and 7. The effect of γ on the birefringence is plotted in Fig. 6. The birefringence of the fiber is large for smaller values of γ and settles down to the value corresponding to that of an

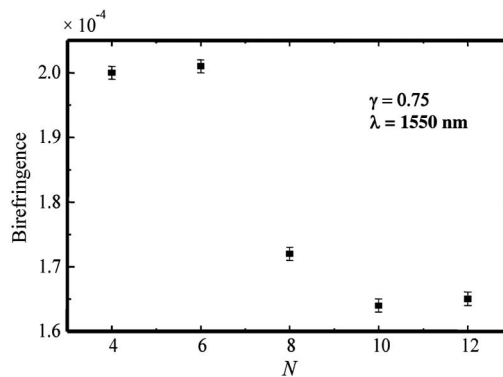


Fig. 7. Effect of number of segments (N) on birefringence of the elliptical SCF.

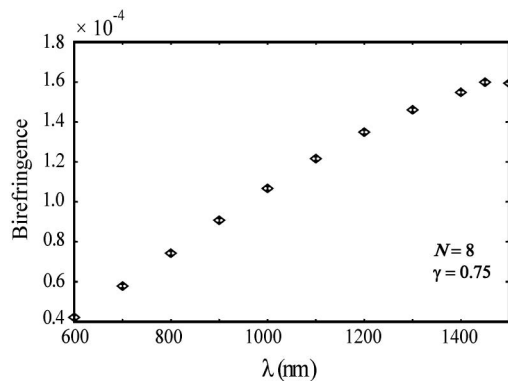


Fig. 8. Spectral variation of the birefringence of the elliptical SCF.

elliptical fiber with uniform cladding as γ increases. In fact, smaller γ corresponds to wider high-index region in the segmented cladding and hence results in an additional geometrical birefringence apart from the already existing birefringence due to the elliptical core. However, this increase is small, and the value of B increases from 1.66×10^{-4} (for $\gamma = 1$) to 2.74×10^{-4} (for $\gamma = 0.35$).

The effect of the number of segments, N , on the birefringence is shown in Fig. 7, where we have plotted B as a function of N for $\gamma = 0.75$. The behavior shown is the result of the interplay between the relative field distribution in high-index segments along the x - and y - axes and the structural asymmetry arising from the values of N . For $N = 4, 8, 12$, there is no structural asymmetry and B decreases with N purely due to the relative field distribution. While for $N = 6, 10, 14$, both the effects are present. A large value of N results in smaller difference in the field amplitudes in high-index segments along the x - and y - axes, and therefore B decreases. When N changes from 4 to 6, the effect of structural asymmetry at $N = 6$ dominates and B slightly increases. However, the change in B is smaller than the accuracy of calculations. The change in B for the entire range of values of N plotted in Fig. 7 is only 17.5%.

We have also studied the effect of the operating wavelength on the birefringence of the SCF, which is shown in Fig. 8. As expected, at longer operating wavelengths, the modal field spreads further into the cladding region, and therefore the effect of the segmented cladding becomes more pronounced. This results in the increase of the value of B with wavelength of operation. However, the effect of the segmented cladding is not significant in the entire range of wavelength where the birefringence increases from 0.4×10^{-4} to 1.6×10^{-4} as the wavelength changes from $0.6 \mu\text{m}$ to $1.5 \mu\text{m}$.

5. Conclusions

We have investigated the modal properties of SCF using a full-vectorial H -field FEM formulation. A circular SCF has been shown to have small birefringence. A highly elliptical SCF with a small core has also been studied to investigate the effect of the segmented cladding on the birefringence. The duty cycle of segmentation and the number of segments have been shown to affect the birefringence of the elliptical SCF only moderately. Hence, fabrication-induced deviations in the segmented cladding parameters would not significantly alter the birefringence of the SCF. Thus, the SCF design is rather robust to fabrication tolerances with respect to birefringence.

This work was partially supported by a UKIERI award titled, "Application-specific microstructured optical fibers."

References

1. V. Rastogi and K. S. Chiang, "Analysis of segmented-cladding fiber by the radial-effective-index method," *J. Opt. Soc. Am. B* **21**, 258–265 (2004).
2. V. Rastogi and K. S. Chiang, "Propagation characteristics of a segmented cladding fiber," *Opt. Lett.* **26**, 491–492 (2001).
3. A. Millo, I. Naeh, and A. Katzir, "Single-mode segmented cladding fibers for middle infrared," *J. Lightwave Technol.* **25**, 2115–2121 (2007).
4. A. Yeung, P. L. Chu, G. D. Peng, K. S. Chiang, and Q. Liu, "Design and fabrication of polymer cross fiber for large-core single-mode operation," *J. Lightwave Technol.* **27**, 101–107 (2009).
5. J. Duan, C. Teng, K. Han, W. Wu, Q. Zhang, and K. S. Chiang, "Fabrication of segmented cladding fiber by bicomponent spinning," *Polym. Eng. Sci.* **49**, 1865–1870 (2009).
6. A. Agrawal, N. Kejalakshmy, J. Chen, B. M. A. Rahman, and K. T. V. Grattan, "Golden spiral photonic crystal fiber: polarization and dispersion properties," *Opt. Lett.* **33**, 2716–2718 (2008).
7. I. K. Hwang, Y. H. Lee, K. Oh, and D. N. Payne, "High birefringence in elliptical hollow optical fiber," *Opt. Express* **12**, 1916–1923 (2004).
8. K. Okamoto, T. Hosaka, and T. Edahiro, "Stress analysis of optical fibres by a finite element method," *IEEE J. Quantum Electron.* **17**, 2123–2129 (1981).
9. N. Kejalakshmy, B. M. A. Rahman, A. Agrawal, T. Wongcharoen, and K. T. V. Grattan, "Characterization of single-polarization single-mode photonic crystal fiber using full-vectorial finite element method," *Appl. Phys. B* **93**, 223–230 (2008).
10. M. Koshiba and K. Saitoh, "Finite element analysis of birefringence and dispersion properties in actual and idealized holey-fiber structures," *Appl. Opt.* **42**, 6267–6275 (2003).
11. Y. C. Liu and Y. Lai, "Optical birefringence and polarization dependent loss of square and rectangular lattice holey fibers with elliptical air holes: numerical analysis," *Opt. Express* **13**, 225–235 (2005).
12. Z. Zhu and T. G. Brown, "Stress induced birefringence in microstructured optical fibers," *Opt. Lett.* **28**, 2306–2308 (2003).
13. B. M. A. Rahman and J. B. Davies, "Finite-element solution of integrated optic waveguides," *J. Lightwave Technol.* **2**, 682–688 (1984).